JGR Space Physics

RESEARCH ARTICLE
10.1029/2018JA026407

Ground-Based Observations of VLF Waves as a Proxy for Satellite Observations: Development of Models Including the Influence of Solar Illumination and Geomagnetic Disturbance Levels

Laura E. Simms[1], Mark J. Engebretson[1], Mark A. Clilverd[2], and Craig J. Rodger[3]

[1]Department of Physics, Augsburg University, Minneapolis, MN, USA, [2]British Antarctic Survey (UKRI-NERC), Cambridge, UK, [3]Department of Physics, University of Otago, Dunedin, New Zealand

Key Points:
- Models accounting for transionospheric absorption and subionospheric attenuation improve satellite-ground VLF PSD correlations
- Validation of these empirical models resulted in correlations between predicted and observed satellite VLF PSD of up to 0.764
- Ground VLF receivers spaced around the Earth could provide longitudinal coverage of outer radiation belt chorus over ±45–75° latitude

Correspondence to:
L. E. Simms,
simmsl@augsburg.edu

Citation:
Simms, L. E., Engebretson, M. J., Clilverd, M. A., & Rodger, C. J. (2019). Ground-based observations of VLF waves as a proxy for satellite observations: Development of models including the influence of solar illumination and geomagnetic disturbance levels. *Journal of Geophysical Research: Space Physics*, *124*, 2682–2696. https://doi.org/10.1029/2018JA026407

Received 16 DEC 2018
Accepted 12 MAR 2019
Accepted article online 18 MAR 2019
Published online 15 APR 2019

Abstract Ground observations of VLF (very low frequency) waves have often been used to infer VLF activity in the magnetosphere; however, they are not an unbiased measure of activity at satellite altitudes due to transionospheric absorption and subionospheric attenuation. We propose several empirical models that control for these effects. VLF power spectral density (PSD) from the VLF/ELF Logger Experiment (VELOX, L=4.6, Halley, Antarctica) is used to predict DEMETER low Earth orbit VLF PSD. Validation correlations of these models are as high as 0.764; thus, ground VLF receivers spaced around the Earth could provide coverage of outer radiation belt lower band chorus over the latitudinal limits of this model (±45–75°). Correlations of four frequency bands (centered at 0.5, 1.0, 2.0, and 4.25 kHz) are compared. The simple linear correlation between ground and satellite VLF PSD in the 1.0-kHz channel was 0.606 (at dawn). A cubic model resulted in higher correlation (0.638). VLF penetration to the ground is reduced by ionospheric absorption during solar illumination and by disruption of ducting field lines during disturbed conditions. Subionospheric attenuation also reduces VLF observations from distant field lines. Addition of these covariates improved predictions. Both solar illumination and disturbed conditions reduced ground observation of VLF PSD, with higher power waves penetrating to the ground proportionately less than lower power waves. The effect of illumination in reducing wave penetration was more pronounced at higher frequency (4.25 kHz), with the effect at a midrange frequency (2.0 kHz) falling between these two extremes.

1. Introduction

Very low frequency (VLF) chorus waves (0.3- to 10-kHz discrete waves) are thought to play an important role in accelerating electrons to damaging relativistic speeds in the radiation belts, with waves in the lower band (0.1–0.5 of the electron cyclotron frequency [fce]) thought to be most effective (Horne & Thorne, 1998; Summers et al., 1998). Several studies have found correlations between lower band chorus and increased relativistic electron flux (Li et al., 2014; MacDonald et al., 2008; Meredith et al., 2002; Rodger et al., 2016; Simms et al., 2018a, 2018b; Smith et al., 2004). Hiss (hundreds of hertz to several kilohertz incoherent waves), on the other hand, is associated with relativistic electron precipitation (Hardman et al., 2015; Hayosh et al., 2013; Lyons et al., 1972; Meredith et al., 2006; Summers et al., 2007; Tsurutani et al., 1975). Thus, any attempts to explain the levels of relativistic electron flux must consider these waves.

However, satellite VLF data, measured in the radiation belts, have not been readily available during much of the time over which radiation belt electron flux data have been collected. For this reason, statistical studies attempting to correlate VLF wave activity with radiation belt electron flux have often used ground-based observations of VLF waves (Simms et al., 2014, 2016; Smith et al., 2004) or proxies based on various measures of the electron population in the radiation belts (Li et al., 2014; MacDonald et al., 2008). Simultaneous observations of VLF chorus events from both satellite and ground stations suggest that ground-observed chorus ought to be a reasonable proxy for satellite observations (Demekhov et al., 2017; Martinez-Calderon et al., 2016; Němec et al., 2016; Titova et al., 2015). Case studies of particle microburst precipitation from the radiation belts also show an association with ground-observed VLF activity (Douma et al., 2018). However, in a statistical study, daily ground-observed VLF activity does not correlate well with electron flux at geosynchronous orbit (Simms et al., 2014, 2016), in comparison to the more robust correlations found between satellite-observed VLF waves and flux (Simms et al., 2018a). In this study, we study the relationship between ground-observed VLF power spectral density (PSD) at Halley, Antarctica, and that observed by the

DEMETER satellite. From this data, we hope to generate a better model for estimating VLF waves occurring in orbit from that observed on the ground.

Waves generated in the magnetosphere are ducted down field-aligned paths to the Halley station at $L \sim 4.6$. (The L value is the distance in Earth radii at which a given magnetic field line crosses the Earth's magnetic equator.) Chorus is most likely to be observed during the dawn period (Golden et al., 2009). At the Halley, Antarctica VELOX (VLF/ELF Logger Experiment) ground station instrument, this dawn peak of chorus occurs at 9–12 UT (6–9 MLT; Smith et al., 2010). The equatorial electron gyrofrequency (fce) at $L = 4.6$ is ~10 kHz (Clilverd et al., 2012), thus lower band chorus that would propagate away from the equator at the geomagnetic latitude of Halley lies between 1 and 5 kHz (0.1–0.5 fce). The ionospheric ducting of VLF waves to the ground is disrupted during ionospheric ionization due to scattering (Lehtinen & Inan, 2009). Absorption due to ionization can occur both during geomagnetic disturbances due to increased auroral electrons (Ozaki et al., 2009) and during periods of solar illumination (Smith et al., 2010). Although these waves, once below the ionosphere, can travel quite far (at least up to 300 km; Ozaki et al., 2008), their spread from distant field lines is reduced by subionospheric attenuation (Challinor, 1967; Smith et al., 2010; Smith & Jenkins, 1998). Both absorption and attenuation are more influential during the day than at night and, therefore, also more influential during the summer months at Halley. The degree to which they act varies with frequency. Both absorption and attenuation act to reduce ground-observed VLF wave power at 1.0 kHz. Subionospheric attenuation has been found to peak in influence around 2–3 kHz, with effects decreasing at higher frequencies (Challinor, 1967; Figure 10.14 of Davies, 1990). However, absorption during periods of solar illumination increases significantly at higher frequencies. This leads to terrestrial influences, such as sferics from lightning, dominating in ground observations above 10 kHz during the day because of the much higher ionospheric absorption in these higher frequencies (Smith et al., 2010), but even at lower frequencies, absorption can have a significant influence. Limiting ground VLF observations to dawn when chorus is seen and to the winter months when there is no solar illumination could, therefore, result in better representation of VLF chorus waves in orbit. A previous study using only dawn observations in winter months from Halley, Antarctica, resulted in a moderate improvement in correlation with electron flux compared to data over the entire year and the full 24-hr period (Simms et al., 2015). While limiting observations to the dawn period allows sampling on a daily basis, limiting data collection to the winter months results in losing data for half the year. This can severely impact the ability to use ground data in studies. There has also been no direct means of assessing exactly how well the ground station observations represent VLF waves in the radiation belt where electron flux is measured.

VLF wave penetration to the ground is thought to be more efficient during quiet geomagnetic periods due to the availability of wave guiding structures and reduced ionospheric attenuation. Disturbed conditions result in the breakup of these structures and thus less efficient ducting of VLF waves to the ground (Gołkowski et al., 2011). Therefore, ground-based VLF observations may be less reliable during the very periods when the VLF waves are most likely to be driving other geomagnetic processes such as electron enhancement and precipitation.

VLF observations from the DEMETER satellite provide an opportunity to establish whether ground-based VLF observations accurately represent the wave activity in orbit. In this study, we determine at which L shell and frequency band the satellite is best correlated with the ground observations as well as how this differs between dayside, nightside, and dawn. Using Halley-observed VLF PSD as the dependent variable in multiple regression, we explore whether solar illumination (responsible for transionospheric absorption), longitudinal separation between satellite and ground (representing subionospheric attenuation), and geomagnetic disturbance level (leading to less efficient ducting and increased absorption) influence the penetration of satellite-observed VLF waves to the ground.

Although correlation analysis does not discriminate between the explanatory and predictor variable, regression analysis makes this distinction. While we use the first set of regression models to determine the influence of predictors on penetration of VLF waves to the ground, these cannot be used as proxy models to predict VLF waves at the altitude of the satellite from ground-observed data. To create predictive models, we must reverse the explanatory and predictor VLF variables, using the satellite data as the dependent variable predicted by the ground data together with the covariates of distance, illumination, and geomagnetic disturbance. We validate these models using a portion of the data held in reserve.

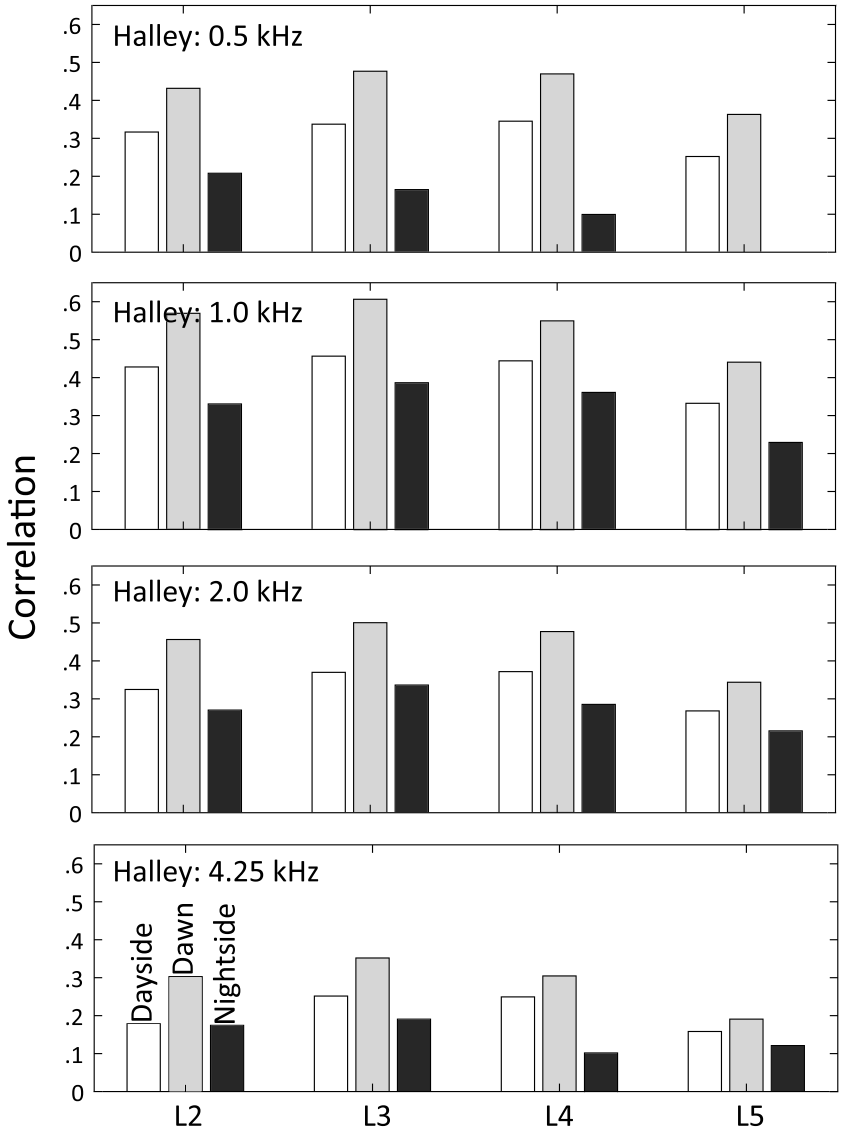

Figure 1. Correlations of Halley (0.5, 1.0, 2.0, and 4.25 kHz channels) with DEMETER VLF. White = dayside (0600–1800 LT Halley; 1030 LT DEMETER); light gray = dawn (0600–0900 MLT Halley; 1030 LT DEMETER); dark gray = nightside (1800–0600 LT Halley; 2230 LT DEMETER).

2. Data and Statistical Methods

Satellite-observed VLF power spectral density (PSD) data (log ($\mu V^2/m^2/Hz$)) were obtained from ICE (Instrument Champ Electrique) on the DEMETER satellite which was in Sun-synchronous orbit 2004–2010 (Berthelier et al., 2006). (We use data from 2004–2007 as this overlaps with observations from the Halley ground station.) Observations from the same frequency bands as the Halley channels (0.5, 1.0, 2.0, and 4.25 kHz) were averaged over each hour and categorized as from the dayside pass of the satellite (10:30 LT) or the nightside pass (22:30 LT). DEMETER was in low Earth orbit, so most observations occurred over McIlwain L shells 2–4, with a lower number of observations at L shell 5. The operation of DEMETER caused no data to be collected at the highest latitudes, severely limiting the higher L coverage. The low Earth polar orbit resulted in limiting observations to roughly ±45–75° latitude over L shells 2–4.

For ground station data, we use the four VLF frequencies from the VELOX (VLF/ELF Logger Experiment) instrument of Halley, Antarctica (L = 4.6) centered at 0.5 kHz (width of 0.5 kHz), 1.0 kHz (width of 1.0 kHz), 2.0 kHz (width of 1.0 kHz), and 4.25 kHz (width of 1.5 kHz). At Halley, below 5 kHz, these waves are

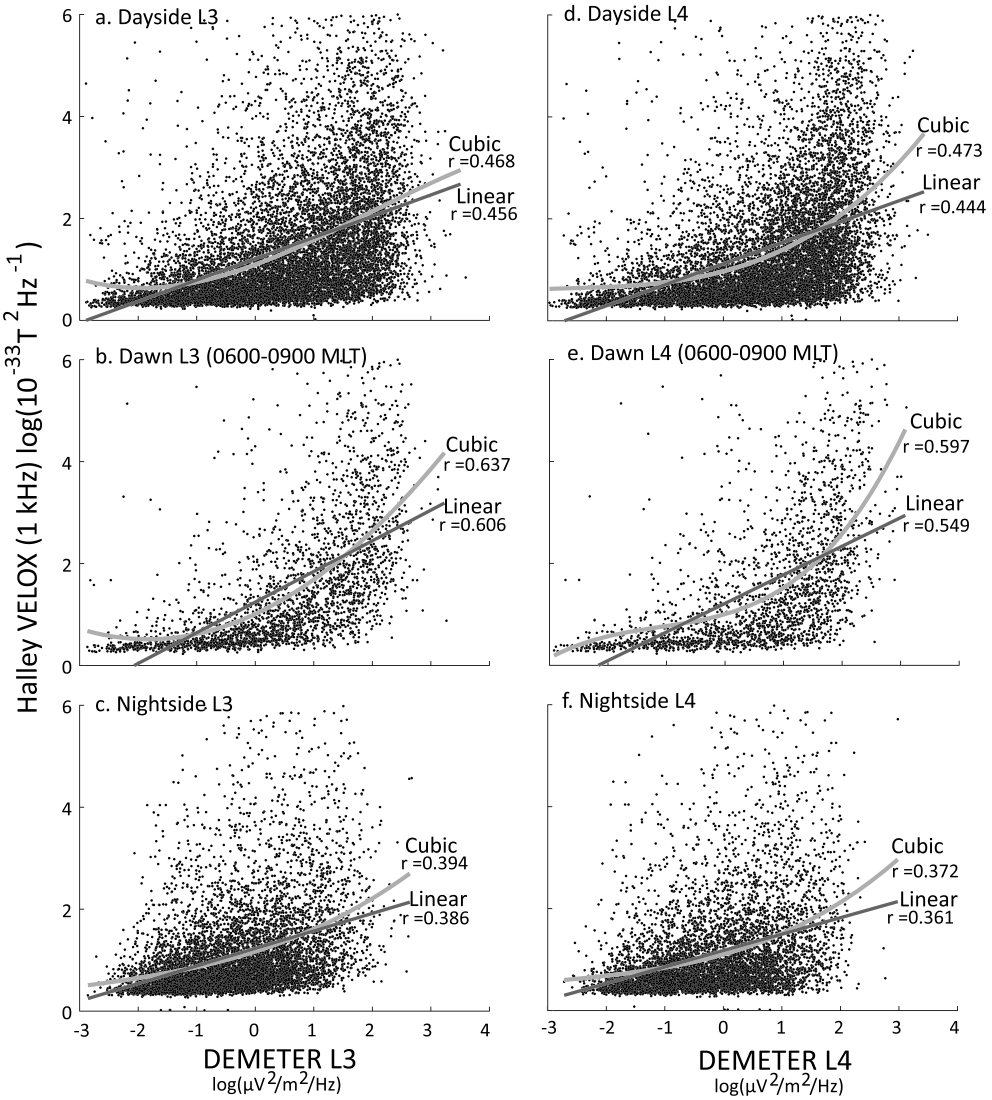

Figure 2. Regression of Halley VELOX data (centered at 1 kHz; 0.5–1.5 kHz) predicted by DEMETER VLF (0.5–1.5 kHz). (a) L3 = dayside (Halley 0600–1800 LT, DEMETER 1030 LT); (b) L3 = dawn (0600–0900 MLT, DEMETER 1030 LT); (c) L3 = nightside (Halley 1800–0600 LT, DEMETER 2230 LT); (d) L4 = dayside; (e) L4 = dawn; (f) L4 = nightside.

predominantly chorus generated in the magnetosphere (Smith et al., 2010). Data were hourly averaged. Isolated observations of >6 mean log PSD (log(10^{-33} T^2/Hz)) were removed from the data set. This corresponds to the upper limit of 60 dB shown in the plots of Smith et al. (2010). To compare to dayside and nightside passes of DEMETER, we use Halley data roughly 6 hr on either side of the satellite pass: 0600–1800 LT and 1800–0600 LT, respectively. This centered the satellite pass within the longitudinal range of Halley as the ground station passed under the satellite. Although the dayside satellite passes were near local noon and the nightside passes near local midnight, at Halley, both of these time periods may be illuminated (during Halley summer) or not illuminated (during Halley winter). The designation of dayside (noon) or nightside (midnight) refers to whether the Earth is oriented toward the sun or away from the sun, respectively. We also specifically model hourly averaged dawn period data from Halley (0600–0900 MLT) when chorus is most likely to be observed (Smith et al., 2010).

Our initial analysis found the highest correlations with Halley ground observations were with DEMETER observations in L3 (L = 3.0–3.99) and L4 (L = 4.0–4.99). We use these L shell ranges (L3 and L4) in the further analyses. As the satellite was rarely exactly over the ground station, magnetic longitude based on

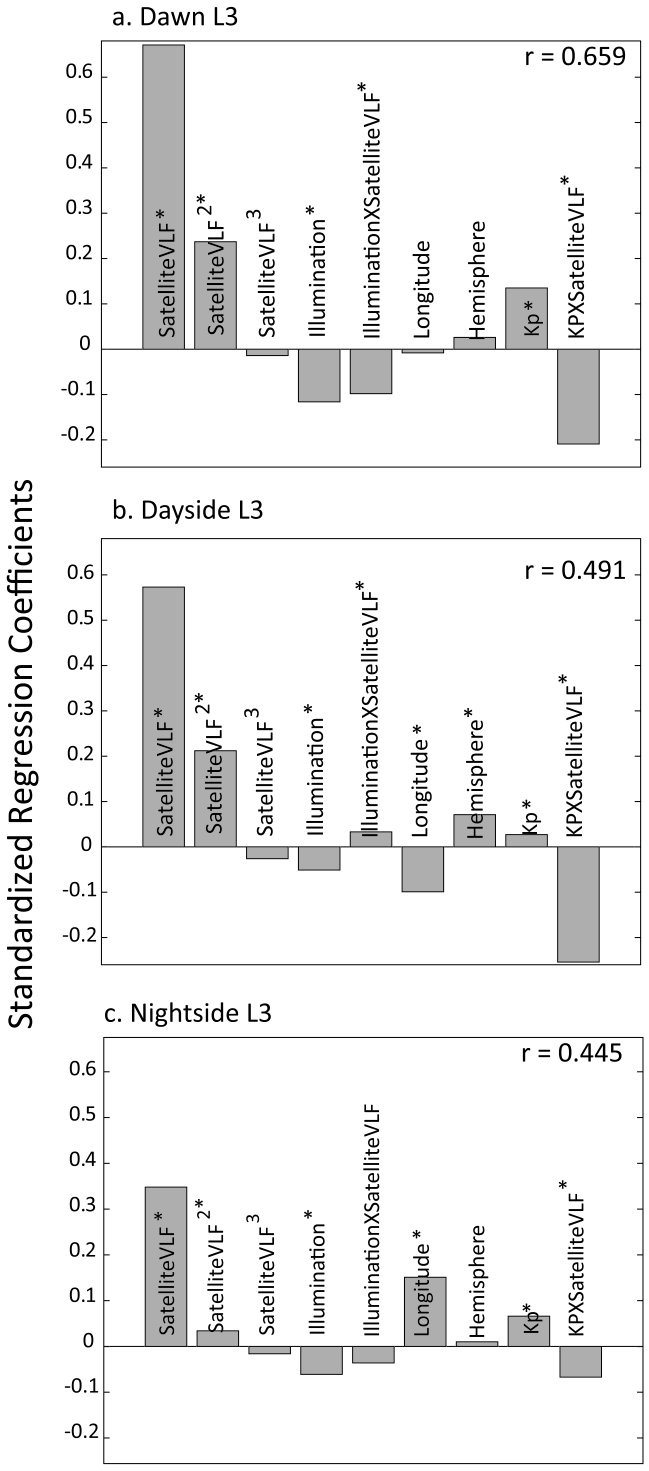

Figure 3. Standardized regression coefficients for models predicting ground Halley VLF activity (1 kHz) from DEMETER VLF, illumination (solar degrees above the horizon at Halley noon), Illumination × DEMETER VLF interaction, hemisphere where DEMETER measurements are taken (south = 1, north = 0), longitudinal separation between Halley and DEMETER, *Kp*, and the *Kp* × DEMETER interaction. (a) Dawn (Halley 0600–0900 MLT; 1 kHz), DEMETER L3; (b) dayside (Halley 0600–1800 LT); and (c) nightside (Halley 1800–0600 LT). Asterisk (*) denotes that coefficient is statistically significant ($p < 0.05$). VLF = very low frequency.

the IGRF (International Geomagnetic Reference Field) model was used to calculate the longitudinal separation (in degrees) of DEMETER from Halley. *Kp* index data (where $Kp > 2.3$ is considered disturbed geomagnetic conditions) were obtained from OMNIWeb.

Solar elevation calculations are summarized in Othman et al. (2018). The multiple regression analyses used are described in Neter et al. (1985). When comparing the effects of predictors on a common scale, standardized regression coefficients are reported from the multiple regressions. To produce standardized coefficients, variances of all variables in the model are standardized to 1. These coefficients then represent how many standard deviations the dependent variable will change when a particular predictor changes by one standard deviation. However, unstandardized coefficients are reported for the final predictive models to allow new predictions of DEMETER data from the ground Halley observations.

Interaction terms in the models were obtained by multiplying parameters. These interaction terms describe the difference response of the predicted variable to one explanatory variable when a second explanatory variable changes in value.

Quadratic and cubic terms were added to models to describe the change in the relationship between ground and satellite observations at varying levels of PSD. At low PSD (<0.5 $\log(10^{-33}$ T^2/Hz) at Halley), the DEMETER satellite is better able to observe signals that are somewhat obscured below the noise floor limit of the Halley VELOX instrument. This may be due to lightning interference or VELOX instrument noise below this level. However, the ground station is still weakly picking up signal below this "noise floor" as there is still some relationship between the ground and satellite observed levels. For example, when ground observations are limited to below this 0.5-kHz threshold, the correlations in the 1.0-kHz channel at L3 ($r = 0.531$) and L4 ($r = 0.441$) between ground and satellite are still considerable. For this reason, we chose not to discard these observations but to describe them. The slope of the relationship, however, changes considerably above the 0.5-kHz noise threshold. For this reason, a simple linear fit over the whole range is not the best model. We find that the addition of quadratic and cubic terms to the regression allows a better fit, with the prediction line curving upward at higher VLF activity to show the changed relationship over this range.

Models predicting DEMETER VLF PSD from Halley observations were produced using years 2004, 2005, and 2007 as the training set. Year 2006 was used to test these models, by correlating observed DEMETER VLF PSD with that predicted by the Halley data. We fit a linear model predicting DEMETER data from Halley VLF observations, a cubic model (using linear, square, and cubic terms of Halley VLF), and a cubic model with covariates (solar illumination and *Kp* along with their interactions with Halley VLF). We present models both with and without longitudinal distance and hemisphere, the latter creating a more global model.

Model fits can be compared using R^2 (coefficient of determination or prediction efficiency), which is the fraction of variation in the data explained by the model. However, for validation we calculated shrinkage by subtracting validation r^2 (correlation between observations and predicted values) from the R^2 of the original regression model. This gave us an estimate of how well the model predicted satellite VLF PSD in a new data set (Muller & Fetterman, 2002).

Table 1
Dawn Models With Standardized Regression Coefficients Predicting Ground VLF (1.0 and 4.25 kHz) From Satellite Observations

Frequency (kHz)	L shell	Model									R^2	r
		DEMETER VLF	DEMETER VLF^2	DEMETER VLF^3	Illumination	Illum × VLF	Longitude	Latitude	*Kp*	*Kp* × VLF		
1	L3	0.606*									0.368	0.606
		0.540*	0.212*	−0.006							0.407	0.637
		0.671*	0.237*	−0.014	−0.116*	−0.088*	−0.008	0.026	0.135*	−0.209*	0.434	0.659
	L4	0.550*									0.302	0.549
		0.326*	0.204*	0.179*							0.357	0.597
		0.369*	0.186*	0.145*	−0.117*	−0.067*	−0.063	0.101*	0.192*	−0.097*	0.390	0.624
4.25	L3	0.352*									0.124	0.352
		0.415*	−0.075*	−0.097*							0.131	0.362
		0.681*	−0.038	−0.156*	−0.315*	−0.215	−0.030	0.113*	0.087*	−0.182*	0.215	0.463
	L4	0.305*									0.093	0.305
		0.246*	−0.013	0.059							0.094	0.306
		0.485*	0.025	−0.030	−0.323*	−0.156*	−0.085*	0.136*	0.113*	−0.136*	0.187	0.432

Note. Prediction efficiency (R^2, fraction of variation in data explained by the regression model) and correlations (r) are given. VLF = very low frequency wave PSD.
*Statistically significant coefficient ($p < 0.05$).

Statistical analyses were performed in IBM SPSS Statistics and MATLAB.

3. Results

Over the DEMETER L range from L2 to L5, in the 1.0-kHz band, VLF PSD dayside satellite observations correlate best with ground-based dawn observations (0600–900 MLT), with correlations ranging from 0.44–0.61 depending on the L shell (Figure 1). Overall dayside correlations (0600–1800 LT) were somewhat lower (0.33–0.46). Nightside observations (1800–0600 LT) showed even lower correlations (0.20–0.39). As expected, satellite data from L4 correlate well with observations from the ground station which lies at $L \sim 4.6$. However, the correlations of L3 DEMETER with Halley are all somewhat higher than the L4 correlations. Satellite and ground observations correlate less well in the 0.5, 2.0, and 4.25 kHz bands. (At 0.5 kHz, L5, nightside, the bar is missing because the correlation was nearly zero.)

3.1. Halley VELOX 1.0-kHz Channel

We continue building our models with the 1.0-kHz L3 and L4 observations. Lines predicting VLF PSD levels observed by the Halley VELOX 1.0-kHz channel (ground station) from DEMETER L3 and L4 VLF PSD (satellite) are presented in Figure 2. We use least squares regression to fit a linear model:

$$\text{Halley} = b_0 + b_1 \times \text{DEMETER}, \tag{1}$$

and a cubic model:

Table 2
Dayside Models With Standardized Regression Coefficients Predicting Ground VLF (1.0 kHz) From Satellite Data

L shell	Model									R^2	r
	DEMETER VLF	DEMETER VLF^2	DEMETER VLF^3	Illumination	Illum × VLF	Longitude	Latitude	*Kp*	*Kp* × VLF		
L3	0.457*									0.209	0.457
	0.465*	0.118*	−0.058*							0.219	0.468
	0.573*	0.212*	−0.026	−0.051*	0.033*	−0.099*	0.073*	0.027*	−0.254*	0.241	0.491
L4	0.444*									0.197	0.444
	0.328*	0.163*	0.058*							0.224	0.473
	0.374*	0.235*	0.089*	−0.049*	0.064*	−0.045*	0.079*	0.059*	−0.222*	0.240	0.490

(*Note*. Prediction efficiency (R^2, fraction of variation in data explained by the regression model) and correlations (r) are given. VLF = very low frequency wave PSD.)
*Statistically significant coefficient ($p < 0.05$).

Table 3
Nightside Models With Standardized Regression Coefficients Predicting Ground VLF (1.0 kHz) From Satellite Observations

L shell	Model									R^2	r
	DEMETER VLF	DEMETER VLF^2	DEMETER VLF^3	Illumination	Illum × VLF	Longitude	Latitude	*Kp*	*Kp* × VLF		
L3	0.387*									0.149	0.386
	0.410*	0.091*	0.021							0.155	0.394
	0.569*	0.109*	0.009	−0.136*	0.024*	0.120*	0.018	−0.108*	−0.174*	0.198	0.445
L4	0.361*									0.130	0.361
	0.365*	0.098*	0.026							0.139	0.373
	0.527*	0.106*	0.040	−0.158*	−0.003	0.131*	0.050*	−0.084*	−0.197*	0.182	0.426

Note. Prediction efficiency (R^2, fraction of variation in data explained by the regression model) and correlations (r). VLF = very low frequency wave PSD.
*Statistically significant coefficient ($p < 0.05$).

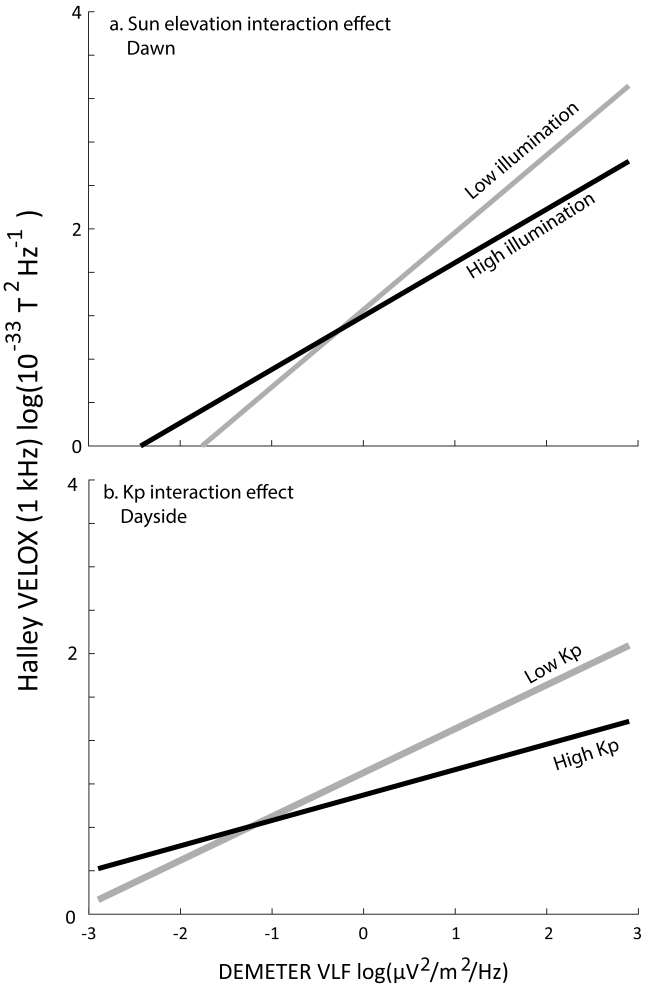

Figure 4. Graphical representation of the interaction terms. (a) Linear relationship between satellite (DEMETER, L3) and dawn ground (Halley, 0600–0900 MLT) VLF when the Sun elevation is less than the median (<5.9° above horizon, gray line) and greater than the median (>5.9° above horizon, black line). (b) Relationship between DEMETER (L3) and dayside ground (Halley, 0600–1800 LT) VLF when $Kp < 2.3$ (gray) and >2.3 (black).

$$\text{Halley} = b_0 + b_1\times\text{DEMETER} + b_2\times\text{DEMETER}^2 + b_3\times\text{DEMETER}^3. \quad (2)$$

The cubic terms capture some of the nonlinear relationship between ground and satellite observations. This allows including Halley VELOX measurements below the 0.5-kHz noise floor in the model. Correlation coefficients for both models are reported. While the correlation for the linear model is the usual Pearson's r, the model correlation of the cubic model is the square root of the R^2 (coefficient of determination).

The linear correlations between dayside Halley and DEMETER of 0.456 (L3, Figure 2a) and 0.444 (L4, Figure 2d) are both improved if the observations are limited to the dawn period when chorus is most strongly seen. Correlations in the dawn period are 0.606 and 0.549 for L3 and L4, respectively (Figures 2b and 2e). Nightside correlations are not as high (0.386 and 0.361 for L3 [Figure 2c] and L4 [Figure 2f]). Cubic models fit the data somewhat better for all categories. For the dawn period, the cubic model correlation is raised to 0.637 (L3) and 0.597 (L4).

A correlation above 0.6 shows we have a reasonable empirical representation of the relationship between ground and satellite data. However, by including more physical processes, we may be able to improve this proxy measure. As VLF wave occurrence is not a global phenomenon, satellite and ground station may see different localized activity when they are far apart. To correct for this possibility, we add longitudinal separation between satellite and ground station as well as the satellite hemisphere to the cubic model. Hemisphere is coded as +1 for south (i.e., the same as Halley) versus −1 for north. In addition, there are likely to be factors that create an observation bias at the ground station. Solar illumination, due to increased ionospheric absorption, and disturbed conditions may both restrict the ducting of waves to the ground station. This would result in lower VLF activity seen at the ground versus the satellite during summer months and periods of high geomagnetic activity. To correct for this, we add the Sun's elevation and *Kp* to the models. However, it is possible that low VLF activity does not penetrate to the ground as effectively as high activity during periods of illumination or disturbance. This could lead to further bias in VLF observations during these periods. To study this, we also add interaction terms to the regression model. These are obtained by multiplying the explanatory factors (e.g., Illumination and Halley VLF PSD). A positive significant effect of this factor would

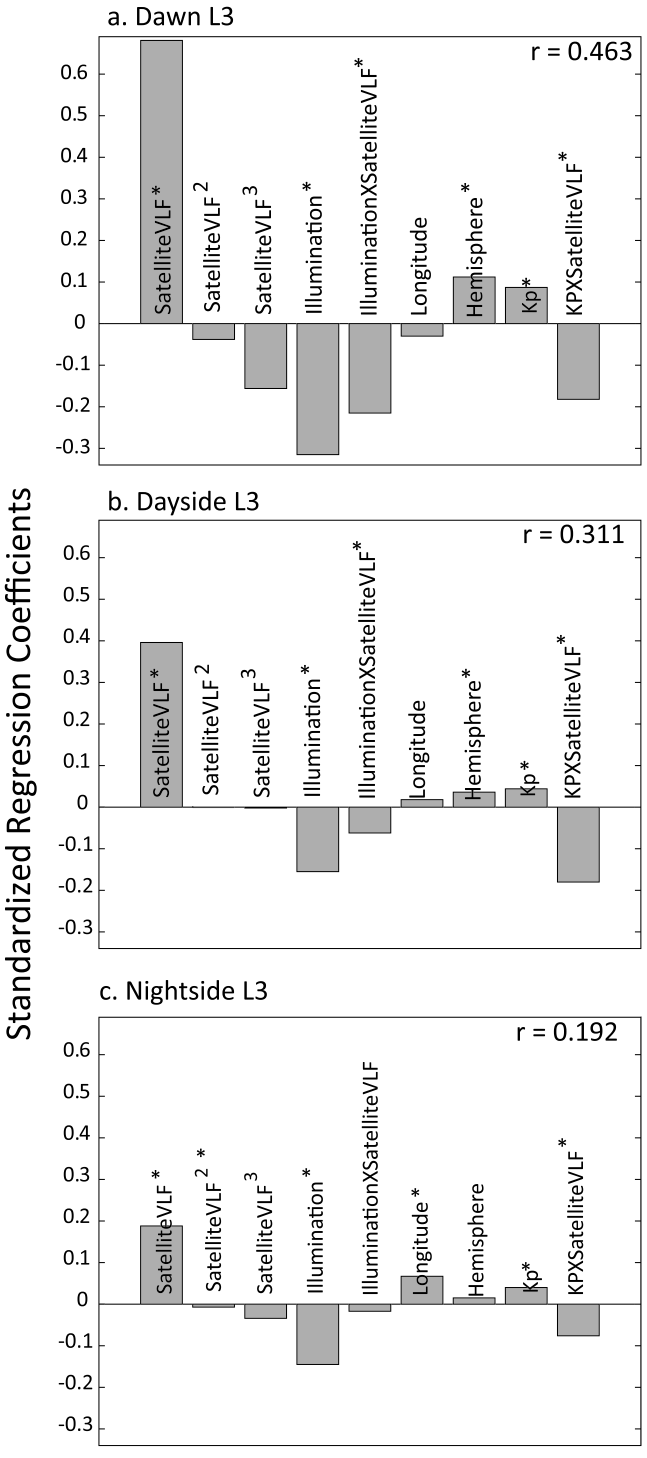

Figure 5. Standardized regression coefficients for models predicting ground Halley VLF activity (4.25 kHz) from DEMETER VLF, illumination (solar degrees above the horizon at Halley noon), Illumination × DEMETER VLF interaction, hemisphere where DEMETER measurements are taken (south = 1, north = 0), longitudinal separation between Halley and DEMETER, *Kp*, and the *Kp* × DEMETER interaction. (a) Dawn (Halley 0600–0900 MLT; 1 kHz), DEMETER L3; (b) dayside (Halley 0600–1800 LT); and (c) Nightside (Halley 1800–0600 LT). Asterisk (*) denotes that coefficient is statistically significant ($p < 0.05$).

indicate that higher VLF activity is predicted at DEMETER by one of these factors when the other is high. The full multifactor model we test is

$$\begin{aligned}\text{Halley} = {} & b_0 + b_1\times\text{DEMETER} + b_2\times\text{DEMETER}^2 + b_3\times\text{DEMETER}^3 \\ & + b_4\times\text{Illumination} + b_5\times\text{Illumination}\times\text{DEMETER} \\ & + b_6\times\text{Longitude} + b_7\times\text{Longitude}\times\text{DEMETER} \\ & + b_8\times\text{Hemisphere} + b_9\times Kp \\ & + b_{10}\times Kp\times\text{DEMETER}.\end{aligned} \tag{4}$$

The standardized regression coefficients in Figure 3 (dawn only; L3: Figure 3a, L4: Figure 3b) show that the most important factor is the linear component of satellite VLF PSD. However, the significant square term of VLF shows that the relationship becomes stronger at higher VLF activity.

The additional variables increase the dawn cubic model correlations to $r = 0.659$ (L3) and 0.624 (L4; standardized regression coefficients of Figure 3 and Table 1). They also improve the correlation over the whole dayside (Table 2: $r = 0.491$ [L3] and 0.490 [L4]) and the nightside (Table 3: 0.445 [L3] and 0.426 [L4]). Analysis of residual errors (plotting residuals vs. predicted values and a normal probability plot) showed that residuals were both randomly and normally distributed. This is confirmation that this model fits the data reasonably well.

Although the addition of more variables offers only a moderate improvement in the fit of the model, it does provide information about the influence of these covariates. Solar illumination is associated with lower VLF activity seen at the ground in both L3 and L4 on both nightside and dayside (Tables 2 and 3), although this effect is seen most strongly during dawn (Table 1 and Figures 3a and 3b). However, this may represent a seasonal effect in addition to representing a possible reduction in wave penetration to the ground station due to ionospheric attenuation. To further explore whether high illumination reduces the efficiency of the ducting of waves to the ground, we add an interaction term (Illumination × DEMETER VLF). In the regression model, this compares the slope of the relationship between satellite and ground VLF under conditions of high and low illumination. In the dawn period at both L3 and L4, the negative Illumination × DEMETER VLF interaction term demonstrates that high illumination impedes the penetration of the highest VLF activity to the ground more than it impedes lower VLF activity. This is graphically described by the interaction plot (Figure 4a) where there is a stronger relationship (higher slope) between satellite and ground VLF (L3) at the lower 50% of illumination (observations below the median solar elevation of 5.9°). A smaller proportion of the dawn satellite VLF activity reaches the ground when both VLF activity and illumination are strong.

The distance of the satellite from the ground station can be measured by longitudinal separation between the two and by whether the satellite is in the same (southern) or different (northern) hemisphere from Halley. We hypothesized that this might account for some of the difference between ground and satellite VLF measurements attributable to subionospheric attenuation. Increased longitudinal separation between satellite and ground had no effect on VLF activity seen at the ground station in the dawn period at L3 (Figure 3a). This may only be because longitudinal distance was less variable during the dawn period as the satellite was passing over the ground station at about the same distance in every

Table 4
Dawn Models With Unstandardized Regression Coefficients for Calculation of Predicted Satellite Observations From Ground VLF (1.0 kHz)

L shell	Model										R^2 coefficient of determination	r validation correlation	Shrinkage $R^2 - r^2$
	Intercept	Halley VLF	Halley VLF^2	Halley VLF^3	Illumination	Illum × VLF	Kp	Kp × VLF	Longitudinal distance	Hemisphere			
L3	−0.3759*	0.6129*									0.369	0.603	0.005
	−1.851*	3.178*	−0.9207*	0.08470*							0.526	0.709	0.023
	−1.877*	3.221*	−0.9319*	0.08562*	0.0008651	−0.001349					0.528	0.707	0.028
	−1.890*	2.699*	−0.8040*	0.07504*	−0.002478	−0.002437	0.02926*	0.0006072			0.598	0.764	0.014
	−1.923*	2.735*	−0.8296*	0.07870*	−0.001059	−0.003355*	0.02775*	0.0010580	−0.00000541	−0.07420*	0.589	0.765	0.004
L4	−0.167	0.5403*									0.318	0.517	0.051
	−1.416	2.731*	−0.8084*	0.07764*							0.430	0.630	0.033
	−1.356	2.738*	−0.8126*	0.07802*	−0.004007	−0.0005874					0.433	0.628	0.039
	−1.350	2.363*	−0.7300*	0.07119*	−0.006792*	−0.001669	0.01959*	0.001696			0.477	0.657	0.045
	−1.301*	2.371*	−0.7340*	0.07158*	−0.006822*	−0.001632	0.01934*	0.001782	−0.0002462	−0.05365	0.479	0.656	

Note. Year 2006 was withheld as the test set. Validation correlations (r) between very low frequency (VLF) predicted by each model and observations from the test set are given. Shrinkage is the difference between the coefficient of determination (R^2) from the predictive model minus the square of the validation correlation (r^2) and quantifies the difference in variation explained by the model in the training set versus that in the test set.
*Statistically significant coefficient ($p < 0.05$).

observation. On the dayside, longitudinal separation did lower the VLF PSD seen on the ground (Figure 3b). Longitudinal separation apparently increased the observed ground VLF PSD on the nightside (Figure 3c). It may be that the satellite, passing over near midnight, sees less VLF activity than the ground station if it is near dusk or dawn.

At lower frequency (1 kHz), on the nightside and at dawn, satellite hemisphere had no effect in the regression. DEMETER observed waves seen by the southern hemisphere ground station were at the same level even when the satellite was over the northern hemisphere. This is expected as the source of the VLF waves is likely near the geomagnetic equator and will propagate equally toward both hemispheres. However, on the dayside overall, when DEMETER was in the same hemisphere as the ground station, VLF activity on the ground was somewhat more highly correlated with satellite observations when the satellite was in the same (southern) hemisphere. This is somewhat unexpected, given that equatorially produced VLF waves are assumed to propagate equally north or south of the equator. This suggests, instead, that there may be some inhomogeneity in wave propagation.

Periods of geomagnetic disturbance ($Kp > 2.3$) resulted in higher VLF activity, with a stronger effect in the dawn period. The interaction term was negative on both dayside and nightside (Figure 3 and Tables 1–3), with high Kp and high satellite VLF PSD resulting in lower ground-observed VLF PSD than would have been predicted by each of these factors individually (dayside: Figure 4b). This interaction shows the disruption of ducting efficiency to the surface during periods of high geomagnetic activity, as well as potentially increased D-region absorption due to energetic electron precipitation from the outer radiation belt (Neal et al., 2015).

3.2. Halley VELOX 4.25-kHz Channel

The 4.25-kHz channel at Halley correlates less well with DEMETER observations than the 1.0-kHz channel (Figure 1). Overall, the relationship between satellite and ground VLF PSD is more linear. Quadratic and cubic terms are not as strong (Figure 5). This is due to the noise floor at this frequency being less of a factor. However, at dawn, relative to other factors at this frequency, solar illumination more strongly reduces the VLF PSD levels seen on the ground due to greater ionospheric absorption (Smith et al., 2010). On the nightside, as at the lower frequency, waves are more likely to be seen at greater longitudinal distance, but this is effect is not as strong. For reasons that are not understood, the response at higher frequency (4.25 kHz) to hemisphere was different. At this higher frequency, at dawn, VLF activity on the ground was more highly correlated with satellite observations when the satellite was in the same (southern) hemisphere. A similar analysis of the 3.0-kHz channel (not shown) showed a response to illumination and distance midrange between the 1.0- and 4.25-kHz results.

3.3. Use of Ground Data as a Proxy for Satellite VLF

Because of the scarcity of satellite VLF data (as described in section 1), ground data have often been used as a proxy for VLF activity in orbit (as described in section 1). While the above models describe how various factors affect the VLF wave penetration from satellite orbit to the ground station, we may be interested in the opposite question: How well VLF activity measured at the Halley ground station can be used to represent satellite activity. As we have shown above, the linear correlation between ground and satellite can be improved by using a cubic

Table 5
Dayside Models With Unstandardized Regression Coefficients for Calculation of Predicted Satellite Observations From Ground VLF (1.0 kHz)

L shell	Model									R^2 coefficient of determination	r validation correlation	Shrinkage $R^2 - r^2$
	Intercept	Halley VLF	Halley VLF^2	Halley VLF^3	Illumination	Illum × VLF	*Kp*	*Kp* × VLF	Longitudinal distance	Hemisphere			
L3	−0.1806	0.4951*									0.203	0.468	−0.016
	−1.313*	2.511*	−0.7400*	0.06854*							0.298	0.545	0.001
	−1.243*	2.480*	−0.7376*	0.06830*	−0.00634*	0.002404*					0.300	0.541	0.007
	−1.487*	1.849*	−0.5641*	0.05310*	−0.00924*	0.002031*	0.039670*	0.001312			0.485	0.682	0.020
	−1.543*	1.780*	−0.5458*	0.05188*	−0.00906*	0.001933*	0.004052*	0.001110	0.0007454*	−0.1081*	0.481	0.687	0.009
L4	−0.05233*	0.4690*									0.193	0.451	−0.010
	−0.9906*	2.344*	−0.7031*	0.06711*							0.275	0.532	−0.008
	−0.8872*	2.293*	−0.6947*	0.06160*	−0.00902*	0.003128*					0.279	0.528	0.0002
	−1.097*	1.766*	−0.5475*	0.05314*	−0.01223*	0.003175*	0.03590*	0.0008672			0.422	0.628	0.028
	−1.002*	1.783*	−0.5569*	0.05420*	−0.01226*	0.002865*	0.03309*	0.0011530	−0.001162*	−0.03135*	0.426	0.631	

Note. Year 2006 was withheld as the test set. Validation correlations (r) between very low frequency (VLF) predicted by each model and observations from the test set are given, along with the shrinkage: the difference in variation explained by the model in the training set versus that in the test set.
*Statistically significant coefficient ($p < 0.05$).

model and adding other variables. In this section we compare several models predicting satellite observations from ground observations.

To produce a predictive model of satellite VLF PSD, we reverse the predictor and response variable in the regression models. We now predict satellite (DEMETER) VLF activity with ground (Halley) VLF activity using four models: (1) simple correlation, (2) cubic regression, (3) cubic regression with the additional covariates of solar illumination and the illumination × VLF interaction, and (4) cubic regression with solar illumination, the illumination × VLF interaction, *Kp*, and the *Kp* × VLF interaction. We do not use longitudinal distance or hemisphere because we wanted to make a more general prediction. We withhold year 2006 as the test set and produce the models using the other years. We report the unstandardized coefficients and R^2 (coefficient of determination or prediction efficiency) of these models (dawn: Table 4; dayside: Table 5; nightside: Table 6). The relative influence of these predictors cannot be determined from the unstandardized coefficients, but they can be used to calculate predictions for novel data from the unscaled 2006 ground VLF data. These predictions are then correlated with the actual data observed at the satellite for these same observations. R^2 (fraction of variation explained by the original model), validation correlations (correlation between observations in the test set and predictions from the models), and shrinkage (the reduction in predictive power in a test set) are also reported in the tables. The shrinkage in the dawn period models was low, indicating that these models predicted new observations relatively well. Some shrinkage statistics during dayside and nightside were negative due to the poorer fit of the models to the training set data.

Scatterplots of observed versus predicted PSD values (dawn, L3, 1.0 kHz) give further indication of how good predictions from Halley are (Figure 6). Predictions from a simple linear model show a correlation of 0.603 with observed values. However, this is not a particularly good model as can be seen by the scatter of points around a line showing the relationship between observed and predicted values (Figure 6a). This simple model does not allow for values much below 0 (satellite VLF PSD lies in the range −3 to 3 $\log(10^{-33}\ T^2/Hz)$). The cubic model is an improvement in correlation ($r = 0.709$) but is unable to predict values below −1 or above 2 (Figure 6b). The addition of only Illumination and the Illumination × VLF interaction did not improve the prediction ability of the cubic model. The correlation between observed and predicted was only 0.707. (This model is given in the tables but is not in the figure.) However, a cubic model with illumination, *Kp*, and their interactions with ground VLF gives an improved fit, with a correlation between predicted and observed values of 0.764 (Figure 6c). The scatter of observed versus predicted points also falls more within the range of actual satellite VLF values. The final model (cubic with additional covariates of illumination, *Kp*, and their interactions with VLF) provides an approximate proxy for what a satellite would observe although it is not exact. Squaring the correlation coefficient of 0.764 gives an r^2 value of 0.584. This means the predicted values of the model explain 58.4% of the variation seen in the observations. Once again, residual error analysis showed the residuals were both randomly and normally distributed.

4. Discussion

The highest correlations between ground and satellite VLF PSD are seen in the 1.0-kHz band over L2 to L4, but it is not a perfect one to one correspondence. While there is a statistically significant linear correlation (up to 0.435 on the dayside when the DEMETER satellite is at L3), it can be increased to 0.606 if observations are

Table 6
Nightside Models With Unstandardized Regression Coefficients for Calculation of Predicted Satellite Observations From Ground VLF (1.0 kHz)

L shell	Model	Intercept	Halley VLF	Halley VLF^2	Halley VLF^3	Illumination	Illum × VLF	*Kp*	*Kp* × VLF	Longitudinal distance	Hemisphere	R^2 coefficient of determination	*r* validation correlation	Shrinkage $R^2 - r^2$
L3		−0.8326*	0.4391*									0.140	0.405	−0.024
		−1.641*	1.982*	−0.6194*	0.06082*							0.198	0.476	−0.029
		−1.784*	2.154*	−0.6937*	0.06915*	0.01372*	0.002731					0.208	0.490	−0.032
		−2.034*	2.186*	−0.6692*	0.0659*	0.01090*	0.003533	0.01405*	−0.004226*			0.230	0.506	−0.026
		−1.991*	2.157*	−0.6463*	0.06327*	0.01714*	0.001876	0.01489*	−0.005069	−0.0009454*	−0.002568*	0.245	0.512	−0.017
L4		−0.6270*	0.4003*									0.119	0.381	−0.026
		−1.250*	1.587*	−0.4685*	0.04500*							0.155	0.427	−0.027
		−1.444*	1.806*	−0.5565*	0.05449*	0.001982*	0.0002783					0.169	0.457	−0.040
		−1.675*	1.893*	−0.5412*	0.05207*	0.01741*	0.001554	0.001263*	−0.006152*			0.182	0.465	−0.034
		−1.506*	1.909*	−.5507*	−.05336*	0.01755*	0.001029	0.01234*	−0.005898*	−0.001605*	−0.1600*	0.200	0.479	−0.029

Note. Year 2006 was withheld as the test set. Validation correlations (*r*) between very low frequency (VLF) predicted by each model and observations from the test set are given, along with the shrinkage: the difference in variation explained by the model in the training set versus that in the test set.
*Statistically significant coefficient ($p < 0.05$).

limited to Halley dawn (UT 9–12), the period during which chorus (coherent VLF) is most likely seen at Halley (Smith et al., 2010). Using a cubic regression further increases the correlation ($r = 0.637$; Figure 2). Nightside correlations are lower than those seen on the dayside.

Although Halley is at L 4.6, DEMETER observations over L2 to L4 all correlate almost equally well with the ground observations. VLF waves are therefore not confined to a specific L shell in orbit, and the Halley ground station would appear to pick up VLF activity from a wider range than its fixed position at $L = 4.6$ would suggest. This is reasonable given the known efficiency of VLF propagation in the Earth-Ionosphere waveguide, particularly equatorward of Halley where ice thickness is low.

VLF waves in the magnetosphere are only observed at ground stations if they are ducted down field-aligned paths. The efficiency of this ducting may be disrupted by solar illumination of the ionosphere (Smith et al., 2010) or during geomagnetically disturbed periods (Gołkowski et al., 2011; Smith et al., 2010). For these reasons, ground data on its own may not be a reliable indicator of VLF activity in the magnetosphere. However, as both these processes are measurable, we built models adding solar degrees above the horizon and *Kp* as covariates in an attempt to improve the correlation between ground and satellite observations. Longitudinal separation between ground and satellite as well as the satellite hemisphere was also added to the models. These additions improved the correlations (up to 0.659 at 1.0 kHz in the dawn period when satellite is at L3; Table 1).

Solar illumination increased transionospheric absorption and was therefore responsible for a reduction in ground VLF PSD relative to that measured at the satellite. This effect was most pronounced at dawn; however, there was a similar, if smaller, response to solar illumination on the nightside. This may be due to contamination of the nightside observations by Halley observations nearer to dawn or dusk. As noted by others, we found that the reduction of VLF waves observed on the ground due to absorption by the sunlit ionosphere is a greater factor at higher frequency (4.25 kHz; Challinor, 1967; Smith et al., 2010; Smith & Jenkins, 1998). However, absorption was not constant over the whole range of VLF values. On the dayside (including dawn), the highest VLF power was less likely to come through to the ground station when illumination was high. Thus, due to absorption, ground observations are not only lower relative to satellite observations, they are also not in constant proportion. This may be because high illumination reduces the distance over which VLF waves can propagate subionospherically. This, in turn, makes the reception of VLF waves at Halley more susceptible to local ionospheric absorption levels during storms, either *F* region storm composition effects or *D* region electron precipitation effects. If VLF wave activity is higher during storms, the system becomes more susceptible to local changes in ionospheric absorption.

While geomagnetic disturbances ($Kp > 2.3$) often lead to higher VLF activity (Smith et al., 2010), the disruption of field lines may reduce the amount of VLF activity seen at the ground as compared to that seen in orbit. As expected, we found higher *Kp* to be associated with more VLF activity, but the negative interaction term between *Kp* and VLF showed that high disturbance preferentially reduced the penetration of the most intense wave activity to the ground. Wave guiding structures appear to be more available in quiet conditions (Gołkowski et al., 2011). In addition, increased ionospheric absorption during geomagnetic disturbances are likely to decrease the efficiency of the coupling between space and ground (Ozaki et al., 2009; Smith et al., 2010).

We measured subionospheric attenuation by including distance (either longitudinal or latitudinal) between ground station and satellite. We hypothesized that when the

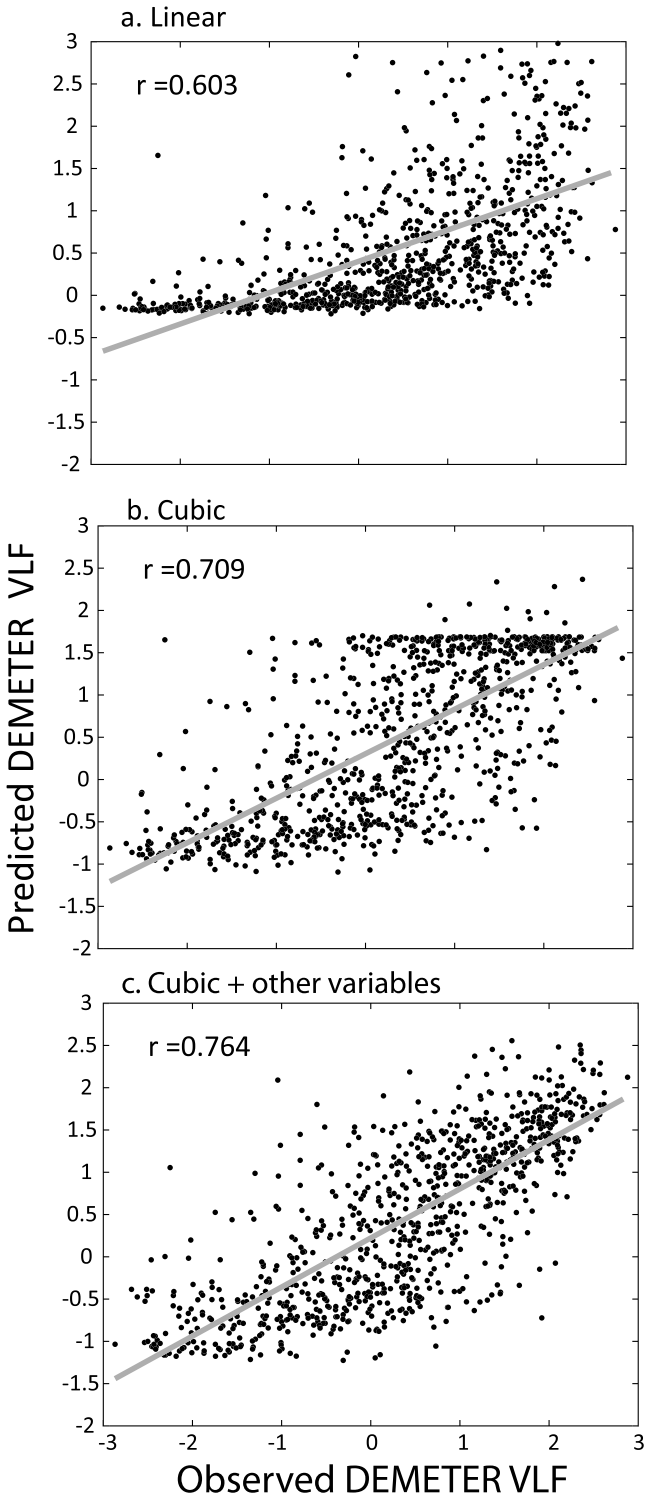

Figure 6. Correlation of DEMETER satellite observations (L3; 0.5–1.5 kHz) with activity predicted by Halley dawn chorus (0600–0900 MLT) and various other parameters. (a) Halley VELOX data linear model; (b) Halley cubic model; and (c) Halley cubic model with solar illumination, *Kp*, and the illumination × VLF and *Kp* × VLF interaction terms. Year 2006 is held out as the test set, while the remaining data are used to produce the model.

satellite was further from the ground station, attenuation would reduce the wave activity seen at the satellite relative to the ground. At greater longitudinal and latitudinal distance, at the lower frequency (1.0 kHz), this effect was seen during the dayside passes. More of the VLF activity seen at the satellite was observed on the ground station both when satellite and ground station were closer longitudinally and when they were in the same hemisphere. This was not the case at the higher frequencies. At 4.25 kHz, longitudinal distance was not a significant factor, and the effect of hemisphere was reduced. At 3.0 kHz (not shown), the attenuation influence due to distance was midway between that observed for 1.0 and 4.25 kHz, both longitudinally and latitudinally. This difference in attenuation effect agrees with observation (Challinor, 1967) that subionospheric attenuation peaks at about 2 kHz and then becomes less influential at higher and lower frequencies. The theoretical reasons for this are discussed by Wait (1957, 2013).

At dawn, we did see a hemisphere effect similar to that for the dayside overall, but there was no longitudinal distance effect. This may be only because the limited time period (UT 9–12) meant the satellite was in much the same longitudinal position over the ground station at every observation. On the nightside, no latitudinal (hemisphere) effect was seen. However, increased longitudinal separation between ground and satellite resulted in higher VLF power readings on the ground. This may be an artifact of the higher VLF power on the dayside. While the ground station may observe higher VLF levels when closer to the dawn or dusk of nightside, the DEMETER satellite, always nearer to midnight on the nightside pass, would not. When the ground station is closer to the dawn or dusk, the satellite (still at midnight) would be at its farthest distance from Halley. Longitudinal distance would be at a maximum just as the ground station is closer to the dayside, making longitudinal distance appears to be a positive influence.

4.1. Ground Data as a Proxy for Satellite Observations

The prediction efficiency (i.e., coefficient of determination or R^2) indicates how closely the data lie along the fitted regression line. It does not provide information on how well the model predicts new observations. For this reason, we perform validation tests of models, withholding year 2006 data as the test set. Although we report the R^2 in the tables, the more important statistic is the correlation between observations and predictions in the test set.

Linear models predicting DEMETER VLF PSD from Halley ground data resulted in reasonable correlations between observed and predicted data (up to 0.603 in the dawn period). However, a cubic model provides a better fit to the test set (up to 0.709), and the addition of covariates not only improves correlation between observed DEMETER VLF PSD and that predicted by the model ($r = 0.764$), it also results in a spread of predicted values that covers more of the natural range of DEMETER VLF observations. The added covariates of solar illumination and the illumination × HalleyVLF interaction account for absorption of VLF waves by the ionosphere and the tendency of higher power VLF to be preferentially absorbed. *Kp* as a covariate accounts for the higher VLF power seen during disturbed conditions, but of more interest to the model, the *Kp* × HalleyVLF interaction accounts for the reduced penetrance of VLF waves to the ground station due to disruption of ducting field lines

during geomagnetic disturbances. (We did not add longitudinal distance or hemisphere to the model in order to make a more generalized prediction.)

While for ULF (ultralow frequency) wave power, *Kp* on its own appears to be a poor proxy (Murphy et al., 2016), and VLF activity shows a correlation with *Kp* (Smith et al., 2010). *Kp* used as a covariate in a proxy model describing satellite VLF PSD from ground VLF data can improve predictions. However, if a VLF proxy was needed for a study designed to determine the effect of *Kp* on VLF waves, the cubic proxy model without covariates could be used with some loss of predictive ability.

As pitch angle scattering by chorus waves is a dominant driver of electron precipitation into the atmosphere, chorus wave amplitudes have also been inferred from low-altitude electron measurements made by Polar Orbiting Environmental Satellites (POES; Li et al., 2013). In this study, predictions from a model based on electron pitch angle distributions of POES electron data correlated well during conjunction events with Van Allen Probes chorus observations, with $r = 0.60$ over a 4-month period in 2012. This is somewhat lower than our validation correlations using dawn or dayside Halley VELOX observations to predict satellite VLF activity ($r = 0.764$ and 0.682, respectively).

Our results suggest that ground VLF receivers spaced around the Earth could provide full longitudinal (MLT) coverage of the satellite environment for lower band chorus in the outer radiation belt. Our models are limited to the ±45–75° latitudinal range where the DEMETER satellite observed L2–4. However, this is similar to the latitudinal range at these L shells of other low Earth polar orbit satellites such as POES. This would make extension of these results possible and could provide a cheaper alternative to the replacement of the POES satellites for VLF wave observation in these latitudes. It is important to note, however, that these models do not extend to the ±15–30° latitude range because processes such as Landau damping and LHR (lower hybrid resonance) reflection, which may limit the propagation of VLF waves both to the ground and to low Earth orbit, are not included in our models (Mourenas et al., 2012).

5. Conclusions

1. Ground VLF PSD observations (Halley, $L \sim 4.6$) are not an unbiased measure of VLF PSD at satellite altitude (DEMETER).
2. Although there is a reasonable linear correlation between the two measures ($r = 0.606$ during the dawn period at Halley, at 1.0 kHz and L3 at DEMETER), this correlation can be improved by correcting for transionospheric absorption during high solar illumination and by accounting for disruption of ducting processes along the field lines during geomagnetic disturbances ($Kp > 2.3$). Adding interaction terms with these covariates also corrected the bias against penetration of high power VLF waves to the ground during conditions of high solar illumination and high geomagnetic disturbance.
3. A full cubic model with added covariates and interactions resulted in a correlation of 0.659 with satellite VLF PSD.
4. A separate model (using a training set) predicting satellite VLF PSD with ground data and the covariates successfully predicted a withheld test set, with a correlation between test set observations and predictions of 0.764 (dawn, L3, 1.0 kHz).
5. Our results suggest that ground VLF receivers spaced around the Earth could provide full longitudinal (MLT) coverage of the satellite environment for lower-band chorus in the outer radiation belt. Although the models presented here are limited in latitudinal range (±45–75°) due to the DEMETER orbit, further models could be built covering the lower latitudes.

Acknowledgments
We thank R. Gamble for preparing and J.-J. Berthelier for providing DEMETER ICE data. All DEMETER data are now available at the CDPP (Centre de données de la Physique des Plasmas) website (cdpp416archive.cnes.fr). Halley VELOX data from BAS are available online (https://data.bas.ac.uk/metadata.php?id=GB/NERC/BAS/AEDC/00055). *Kp* values were obtained from Goddard Space Flight Center Space Physics Data Facility at the OMNIWeb data website (http://omniweb.gsfc.nasa.gov/html/ow_data.html). M. A. Clilverd was supported by the Natural Environmental Research Council grant NE/J008125/1. Work at Augsburg University was supported by NSF grants PLR-1341493 and AGS-1651263.

References

Berthelier, J. J., Godefroy, M., Leblanc, F., Malingre, M., Menvielle, M., Lagoutte, D., et al. (2006). ICE, the electric field experiment on DEMETER. *Planetary and Space Science*, *54*(5), 456–471. https://doi.org/10.1016/j.pss.2005.10.016

Challinor, R. A. (1967). The phase velocity and attenuation of audio-frequency electro-magnetic waves from simultaneous observations of atmospherics at two spaced stations. *Journal of Atmospheric and Terrestrial Physics*, *29*(7), 803–810. https://doi.org/10.1016/0021-9169(67)90046-3

Clilverd, M. A., Rodger, C. J., Danskin, D., Usanova, M. E., Raita, T., Ulich, T., & Spanswick, E. L. (2012). Energetic particle injection, acceleration, and loss during the geomagnetic disturbances which upset Galaxy 15. *Journal of Geophysical Research*, *117*, A12213. https://doi.org/10.1029/2012JA018175

Davies, K. (1990). *Ionospheric radio, IEE electromagnetic waves series, 31*. London, UK: P. Peregrinus.

Demekhov, A. G., Manninen, J., Santolík, O., & Titova, E. E. (2017). Conjugate ground-spacecraft observations of VLF chorus elements. *Geophysical Research Letters*, *44*, 11,735–11,744. https://doi.org/10.1002/2017GL076139

Douma, E., Rodger, C. J., Clilverd, M. A., Hendry, A. T., Engebretson, M. J., & Lessard, M. R. (2018). Comparison of relativistic microburst activity seen by SAMPEX with ground-based wave measurements at Halley, Antarctica. *Journal of Geophysical Research: Space Physics*, *123*, 1279–1294. https://doi.org/10.1002/2017JA024754

Golden, D. I., Spasojevic, M., & Inan, U. S. (2009). Diurnal dependence of ELF/VLF hiss and its relation to chorus at L = 2.4. *Journal of Geophysical Research*, *114*, A05212. https://doi.org/10.1029/2008JA013946

Gołkowski, M., Cohen, M. B., Carpenter, D. L., & Inan, U. S. (2011). On the occurrence of ground observations of ELF/VLF magnetospheric amplification induced by the HAARP facility. *Journal of Geophysical Research*, *116*, A04208. https://doi.org/10.1029/2010JA016261

Hardman, R., Clilverd, M. A., Rodger, C. J., Brundell, J. B., Duthie, R., Holzworth, R. H., et al. (2015). A case study of electron precipitation fluxes due to plasmaspheric hiss. *Journal of Geophysical Research: Space Physics*, *120*, 6736–6748. https://doi.org/10.1002/2015JA021429

Hayosh, M., Pasmanik, D. L., Demekhov, A. G., Santolik, O., Parrot, M., & Titova, E. E. (2013). Simultaneous observations of quasi-periodic ELF/VLF wave emissions and electron precipitation by DEMETER satellite: A case study. *Journal of Geophysical Research: Space Physics*, *118*, 4523–4533. https://doi.org/10.1002/jgra.50179

Horne, R. B., & Thorne, R. M. (1998). Potential waves for relativistic electron scattering and stochastic acceleration during magnetic storms. *Geophysical Research Letters*, *25*(15), 3011–3014. https://doi.org/10.1029/98GL01002

Lehtinen, N. G., & Inan, U. S. (2009). Full-wave modeling of transionospheric propagation of VLF waves. *Geophysical Research Letters*, *36*, L03104. https://doi.org/10.1029/2008GL036535

Li, W., Ni, B., Thorne, R. M., Bortnik, J., Green, J. C., Kletzing, C. A., et al. (2013). Constructing the global distribution of chorus wave intensity using measurements of electrons by the POES satellites and waves by the Van Allen Probes. *Geophysical Research Letters*, *40*, 4526–4532. https://doi.org/10.1002/grl.50920

Li, W., Thorne, R. M., Ma, Q., Ni, B., Bortnik, J., Baker, D. N., et al. (2014). Radiation belt electron acceleration by chorus waves during the 17 March 2013 storm. *Journal of Geophysical Research: Space Physics*, *119*, 4681–4693. https://doi.org/10.1002/2014JA019945

Lyons, L. R., Thorne, R. M., & Kennel, C. F. (1972). Pitch-angle diffusion of radiation belt electrons within the plasmasphere. *Journal of Geophysical Research*, *77*(19), 3455–3474. https://doi.org/10.1029/JA077i019p03455

MacDonald, E. A., Denton, M. H., Thomsen, M. F., & Gary, S. P. (2008). Superposed epoch analysis of a whistler instability criterion at geosynchronous orbit during geomagnetic storms. *Journal of Atmospheric and Solar-Terrestrial Physics*, *70*(14), 1789–1796. https://doi.org/10.1016/j.jastp.2008.03.021

Martinez-Calderon, C., Shiokawa, K., Miyoshi, Y., Keika, K., Ozaki, M., Schofield, I., et al. (2016). ELF/VLF wave propagation at sub-auroral latitudes: Conjugate observation between the ground and Van Allen Probes A. *Journal of Geophysical Research: Space Physics*, *121*, 5384–5393. https://doi.org/10.1002/2015JA022264

Meredith, N. P., Horne, R. B., Glauert, S. A., Thorne, R. M., Summers, D., Albert, J. M., & Anderson, R. R. (2006). Energetic outer zone electron loss timescales during low geomagnetic activity. *Journal of Geophysical Research*, *111*, A05212. https://doi.org/10.1029/2005JA011516

Meredith, N. P., Horne, R. B., Iles, R. H. A., Thorne, R. M., Heynderickx, D., & Anderson, R. R. (2002). Outer zone relativistic electron acceleration associated with substorm-enhanced whistler mode chorus. *Journal of Geophysical Research*, *107*(A7), 1144. https://doi.org/10.1029/2001JA900146

Mourenas, D., Artemyev, A. V., Ripoll, J.-F., Agapitov, O. V., & Krasnoselskikh, V. V. (2012). Timescales for electron quasi-linear diffusion by parallel and oblique lower-band chorus waves. *Journal of Geophysical Research*, *117*, A06234. https://doi.org/10.1029/2012JA017717

Muller, K. E., & Fetterman, B. A. (2002). *Regression and ANOVA: An integrated approach using SAS software* (p. 575). Cary, NC: SAS Institute, Inc.

Murphy, K. R., Mann, I. R., Rae, I. J., Sibeck, D. G., & Watt, C. E. J. (2016). Accurately characterizing the importance of wave-particle interactions in radiation belt dynamics: The pitfalls of statistical wave representations. *Journal of Geophysical Research: Space Physics*, *121*, 7895–7899. https://doi.org/10.1002/2016JA022618

Neal, J. J., Rodger, C. J., Clilverd, M. A., Thomson, N. R., Raita, T., & Ulich, T. (2015). Long-term determination of energetic electron precipitation into the atmosphere from AARDDVARK subionospheric VLF observations. *Journal of Geophysical Research: Space Physics*, *120*, 2194–2211. https://doi.org/10.1002/2014JA020689

Němec, F., Bezděková, B., Manninen, J., Parrot, M., Santolík, O., Hayosh, M., & Turunen, T. (2016). Conjugate observations of a remarkable quasiperiodic event by the low-altitude DEMETER spacecraft and ground-based instruments. *Journal of Geophysical Research: Space Physics*, *121*, 8790–8803. https://doi.org/10.1002/2016JA022968

Neter, J., Wasserman, W., & Kutner, M. H. (1985). *Applied linear statistical models*. Homewood, IL: Richard D. Irwin, Inc.

Othman, A. B., Belkilani, K., & Besbes, M. (2018). Global solar radiation on tilted surfaces in Tunisia: Measurement, estimation and gained energy assessments. *Energy Reports*, *4*, 101–109. https://doi.org/10.1016/j.egyr.2017.10.003

Ozaki, M., Yagitani, S., Nagano, I., Hata, Y., Yamagishi, H., Sato, N., & Kadokura, A. (2008). Localization of VLF ionospheric exit point by comparison of multipoint ground-based observation with full-wave analysis. *Polar Science*, *2*(4), 237–249. https://doi.org/10.1016/j.polar.2008.09.001

Ozaki, M., Yagitani, S., Nagano, I., Yamagishi, H., & Sato, N. (2009). Estimation of enhanced electron density in the lower ionosphere using correlation between natural VLF emission intensity and CNA. *Antarctic Record*, *53*(2), 123–135. https://doi.org/10.15094/00009496

Rodger, C. J., Cresswell-Moorcock, K., & Clilverd, M. A. (2016). Nature's Grand Experiment: Linkage between magnetospheric convection and the radiation belts. *Journal of Geophysical Research: Space Physics*, *121*, 171–189. https://doi.org/10.1002/2015JA021537

Simms, L., Engebretson, M., Clilverd, M., Rodger, C., Lessard, M., Gjerloev, J., & Reeves, G. (2018a). A distributed lag autoregressive model of geostationary relativistic electron fluxes: Comparing the influences of waves, seed and source electrons. *and solar wind inputs. Journal of Geophysical Research: Space Physics*, *123*, 3646–3671. https://doi.org/10.1002/2017JA025002

Simms, L. E., Engebretson, M. J., Clilverd, M. A., Rodger, C. J., Lessard, M. R., & Reeves, G. D. (2018b). Nonlinear and synergistic effects of ULF Pc5, VLF chorus, and EMIC waves on relativistic electron flux at geosynchronous orbit. *Journal of Geophysical Research: Space Physics*, *123*, 4755–4766. https://doi.org/10.1029/2017JA025003

Simms, L. E., Engebretson, M. J., Pilipenko, V., Reeves, G. D., & Clilverd, M. (2016). Empirical predictive models of daily relativistic electron flux at geostationary orbit: Multiple regression analysis. *Journal of Geophysical Research: Space Physics*, *121*, 3181–3197. https://doi.org/10.1002/2016JA022414

Simms, L. E., Engebretson, M. J., Smith, A. J., Clilverd, M., Pilipenko, V. A., & Reeves, G. D. (2014). Prediction of relativistic electron flux following storms at geostationary orbit: Multiple regression analysis. *Journal of Geophysical Research: Space Physics*, *119*, 7297–7318. https://doi.org/10.1002/2014JA019955

Simms, L. E., Engebretson, M. J., Smith, A. J., Clilverd, M., Pilipenko, V. A., & Reeves, G. D. (2015). Analysis of the effectiveness of ground-based VLF wave observations for predicting or nowcasting relativistic electron flux at geostationary orbit. *Journal of Geophysical Research: Space Physics*, *120*, 2052–2060. https://doi.org/10.1002/2014JA020337

Smith, A. J., Horne, R. B., & Meredith, N. P. (2010). The statistics of natural ELF/VLF waves derived from a long continuous set of ground based observations at high latitude. *Journal of Atmospheric and Solar-Terrestrial Physics*, *72*(5-6), 463–475. https://doi.org/10.1016/j.jastp.2009.12.018

Smith, A. J., & Jenkins, P. J. (1998). A survey of natural electromagnetic noise in the frequency range f = 1-10 kHz at Halley station, Antarctica: 1. Radio atmospherics from lightning. *Journal of Atmospheric and Solar-Terrestrial Physics*, *60*(2), 263–277. https://doi.org/10.1016/S1364-6826(97)00057-6

Smith, A. J., Meredith, N. P., & O'Brien, T. P. (2004). Differences in ground-observed chorus in geomagnetic storms with and without enhanced relativistic electron fluxes. *Journal of Geophysical Research*, *109*, A11204. https://doi.org/10.1029/2004JA010491

Summers, D., Ni, B., & Meredith, N. P. (2007). Timescales for radiation belt electron acceleration and loss due to resonant wave-particle interactions: 2. Evaluation for VLF chorus, ELF hiss, and electromagnetic ion cyclotron waves. *Journal of Geophysical Research*, *112*, A04207. https://doi.org/10.1029/2006JA011993

Summers, D., Thorne, R. M., & Xiao, F. (1998). Relativistic theory of wave-particle resonant diffusion with application to electron acceleration in the magnetosphere. *Journal of Geophysical Research*, *103*(A9), 20,487–20,500. https://doi.org/10.1029/98JA01740

Titova, E. E., Kozelov, B. V., Demekhov, A. G., Manninen, J., Santolík, O., Kletzing, C. A., & Reeves, G. (2015). Identification of the source of quasiperiodic VLF emissions using ground-based and Van Allen Probes satellite observations. *Geophysical Research Letters*, *42*, 6137–6145. https://doi.org/10.1002/2015GL064911

Tsurutani, B. T., Smith, E. J., & Thorne, R. M. (1975). Electromagnetic hiss and relativistic electron losses in the inner zone. *Journal of Geophysical Research*, *80*(4), 600–607. https://doi.org/10.1029/JA080i004p00600

Wait, J. R. (1957). The attenuation vs frequency characteristics of VLF radio waves. *Proceedings of the IRE*, *45*(6), 768–771. https://doi.org/10.1109/JRPROC.1957.278470

Wait, J. R. (2013). *Electromagnetic waves in stratified media: Revised edition including supplemented material*. Oxford, UK: Pergamon Press.